ORNL/SPR-2019/1364

Improving Elemental Ratio Measurements on Uranyl Fluoride with NanoSIMS

Andrew Miskowiec
Alex Zirakparvar
Tyler Spano

01/31/2020

Approved for release
Distribution is unlimited

OAK RIDGE NATIONAL LABORATORY
MANAGED BY UT-BATTELLE FOR THE US DEPARTMENT OF ENERGY

ORNL/TM-2019/1364

Nuclear Nonproliferation Division

IMPROVING ELEMENTAL RATIO MEASUREMENTS ON URANYL FLUORIDE WITH NANOSIMS

Andrew Miskowiec
Alex Zirakparvar
Tyler Spano

01/31/2020

Prepared by
OAK RIDGE NATIONAL LABORATORY
Oak Ridge, TN 37831-6283
managed by
UT-BATTELLE, LLC
for the
US DEPARTMENT OF ENERGY
under contract DE-AC05-00OR22725

CONTENTS

FIGURES

TABLES

EXECUTIVE SUMMARY

Measurements on samples of calcined uranyl fluoride (UO_2F_2) using Raman spectroscopy, electron microscopy with elemental analysis, and secondary ion mass spectrometry (SIMS) indicate four facts. First, UO_2F_2 undergoes a previously unreported oxidation reaction beginning around 350 °C in air. The resulting oxidation compound is likely similar to U_3O_8/UO_3, but presently represents a novel chemical species. Second, variations in F/U ratio across samples as measured by electron microscopy with x-ray spectroscopy correlate with variations in F/U ratio as measured with the NanoSIMS 50L instrument. Third, simple mixed powders of LaF_3+U_3O_8 are not sufficiently homogeneous to act as a high F+U content standard material. Fourth, additional method development for determining the bulk F/U ratio using an alternative technique is necessary to further develop analytical standards.

1. INTRODUCTION

Secondary ion mass spectrometry (SIMS) is a workhorse technique in the isotopic analysis community for measuring spatially resolved isotopic ratios. A less common but equally valuable analytical mode of operation in SIMS is elemental ratios: e.g., the ratio of fluorine to uranium in uranyl fluoride. The Nuclear Nonproliferation Division maintains a Cameca NanoSIMS 50L small-geometry SIMS instrument ("NanoSIMS") which is optimized for high spatial resolution and sufficient dynamic range to measure both U isotope ratios and F/U ratios in samples containing ppm-level concentrations of these elements.

In order to optimize the performance of the NanoSIMS instrument for measurement of the F/U ratio (specifically with the goal of determining the F/U ratio in uranyl fluoride (UO_2F_2)) we have pursued a research plan involving two parallel tracks: First, develop new analytical standards with high F and U concentration to act as elemental ratio standards. Second, develop appropriate correction regimes for uranyl fluoride by studying samples with known fluorine concentration.

To wit, it was recently discovered that UO_2F_2 undergoes a hydrolysis reaction in humid environments whereby F is lost, likely in the form of volatile HF, as the material transforms to a uranyl hydroxide. The hydrolysis reaction occurs on the order of days to months, depending on the availability of atmospheric water [relative humidity (RH)] and temperature. At 25 °C and 75% humidity, UO_2F_2 almost completely converts to uranyl hydroxide after 25 days. It is unknown whether the NanoSIMS can be used to measure the F/U ratio in UO_2F_2 as it undergoes this reaction. In order to explore that question, analytical correction regimes must be explored, which requires materials with known F/U ratio (standards) and an understanding of the so-called matrix effect, i.e., the influence of the chemical form itself on the analytical measurement.

In addition, we sought an opportunity to study the oxidation reaction of UO_2F_2 . To our knowledge, no previous studies of the calcination behavior of UO_2F_2 have been reported; but, we speculated, based on experience with other uranium compounds, that UO_2F_2 would likely oxidize to U_3O_8 near 300–500 °C. Our experimental plan was to prepare a series of specimens calcined in air along the temperature range 350–550 °C, interrogate their chemical phase with micro-Raman spectroscopy, measure the elemental F/U concentrations at low resolution using scanning electron microscopy (SEM) with energy dispersive x-ray spectroscopy (EDS), and compare the measured F/U ratio using the NanoSIMS instrument. This set of samples would allow us to simultaneously make progress on the analytical problem of measuring the F/U ratio with NanoSIMS as well as explore an unanswered chemical question (what is the calcination reaction of uranyl fluoride?)

Calcining UO_2F_2 at different temperatures should result in materials with variable F/U ratio as the oxidation reaction proceeds. The resulting materials represent specimens for which it is known that the F/U ratio varies from 2 (for *"ideal"* UO_2F_2). Although the bulk F/U concentration is not known, it is known that it is variable. Previous measurements by us and others have indicated that the F/U ratio as determined by SIMS for UO_2F_2 can be highly variable. It is unknown whether variability is an analytical artefact or if it is a true variation (due to uneven surface oxidation or hydrolysis).

2. EXPERIMENTAL DESIGN

Uranyl fluoride is produced by the hydrolysis of UF_6 ($UF_{6(g)} + 2H_2O_{(g)} \rightarrow 4HF_{(g)} + UO_2F_{2(s)}$). The hydrolysis reaction occurs quickly, and the resulting UO_2F_2 is a solid compound. For these experiments, UO_2F_2 was produced by the hydrolysis of UF_6. UF_6 was flowed into a reaction chamber (glovebox) held at approximately 35% RH (ambient temperature, 21 °C). The particulate UO_2F_2 was collected on a set of Teflon-based laminate mats and concentrated. The stock UO_2F_2 for these experiments was used as is

without further purification. Stock UO_2F_2 was prepared in April 2019 for experiments beginning in July 2019. Raman spectra of the initial material showed that the powder was likely as anhydrous UO_2F_2, a common chemical form that is stable at low humidity.

Table 1 lists the calcination schedule of each sample. Specimens were calcined in a DSC600 temperature stage under a controlled atmosphere of 790 Pa water vapor (25% RH at 25 °C) in Al crucibles. The temperature was increased at a rate of 15 °C/min to the calcination temperature, held for 60 min, and cooled without temperature control to ambient temperature. Raman spectra were collected before and after calcination.

Table 1. Calcination schedule for UO_2F_2 specimens.

Sample designation	Calcination temperature	Calcination time	Water vapor pressure
S0	550 °C	60 min	790 Pa
S1	350 °C	60 min	790 Pa
S2	400 °C	60 min	790 Pa
S3	450 °C	60 min	790 Pa
S4	500 °C	60 min	790 Pa
S5	500 °C	60 min	790 Pa
S6	525 °C	60 min	790 Pa

3. RAMAN SPECTROSCOPY

Raman spectra were collected before and after calcination. All samples had identical Raman spectra prior to measurement (corresponding to anhydrous UO_2F_2), and we omit those results here. In Figure 1 we show prototypical Raman spectra (collected with 532 nm laser for approximately 300 s with 0.26 μW power focused over 0.7569 μm^2 area) after calcination of each sample as well as optical images before (middle column) and after (rightmost column). A clear continuation in color change is associated with the growth of a band of scattering features peaked near 680 cm^{-1}. Measured in S0, the Raman spectra changes again, showing a spectrum that is remarkably similar, qualitatively, to U_3O_8, but with spectral features blueshifted approximately 165 cm^{-1}.

Sample S1, with peaks centered at 914, 180, and 440 cm^{-1}, is representative of anhydrous uranyl fluoride. Only a small peak of the second phase at 680 cm^{-1} is present in S1, indicating that S1 is primarily still uranyl fluoride. In S2, at 400 °C, the dominant feature is the second phase at 680 cm^{-1}, but a small amount of scattering intensity at 914 cm^{-1} indicates an incomplete conversion of UO_2F_2. At 450 °C (S3), the spectrum is dominated by the intermediate phase and no scattering intensity at 914 cm^{-1} is observed. The spectrum collected at 550 °C (S0) is qualitatively distinct from the other samples. The spectrum itself has a distinct triplet massif centered near 580 cm^{-1}, which is composed of two broad sidebands. Additional, weaker, peaks are observed at 400, 230, 125, 780, and 820 cm^{-1}. Most noteworthy about the spectrum of S0 is its structural similarity to the Raman spectra of U_3O_8 (Figure 2). The spectrum of U_3O_8 is generally sharper and more well-defined, but also redshifted approximately 165 cm^{-1} compared to the collected spectrum. However, this similarity is highly suggestive of a chemical pathway involving the formation of U_3O_8.

We speculate that the intermediate phase that includes the main peak at 680 cm^{-1} is structurally similar to amorphous UO_3, a speculation based on ongoing measurements of amorphous UO_3 under pressure. If such a chemical path is correct, the proposed chemical reaction could proceed as: $2UO_2F_2 + O_2 \rightarrow 2UO_3 +$

$2F_2$ and $6UO_3$ -> $2U_3O_8 + O_2$. As far as we are aware, this reaction has not yet been elucidated in the literature.

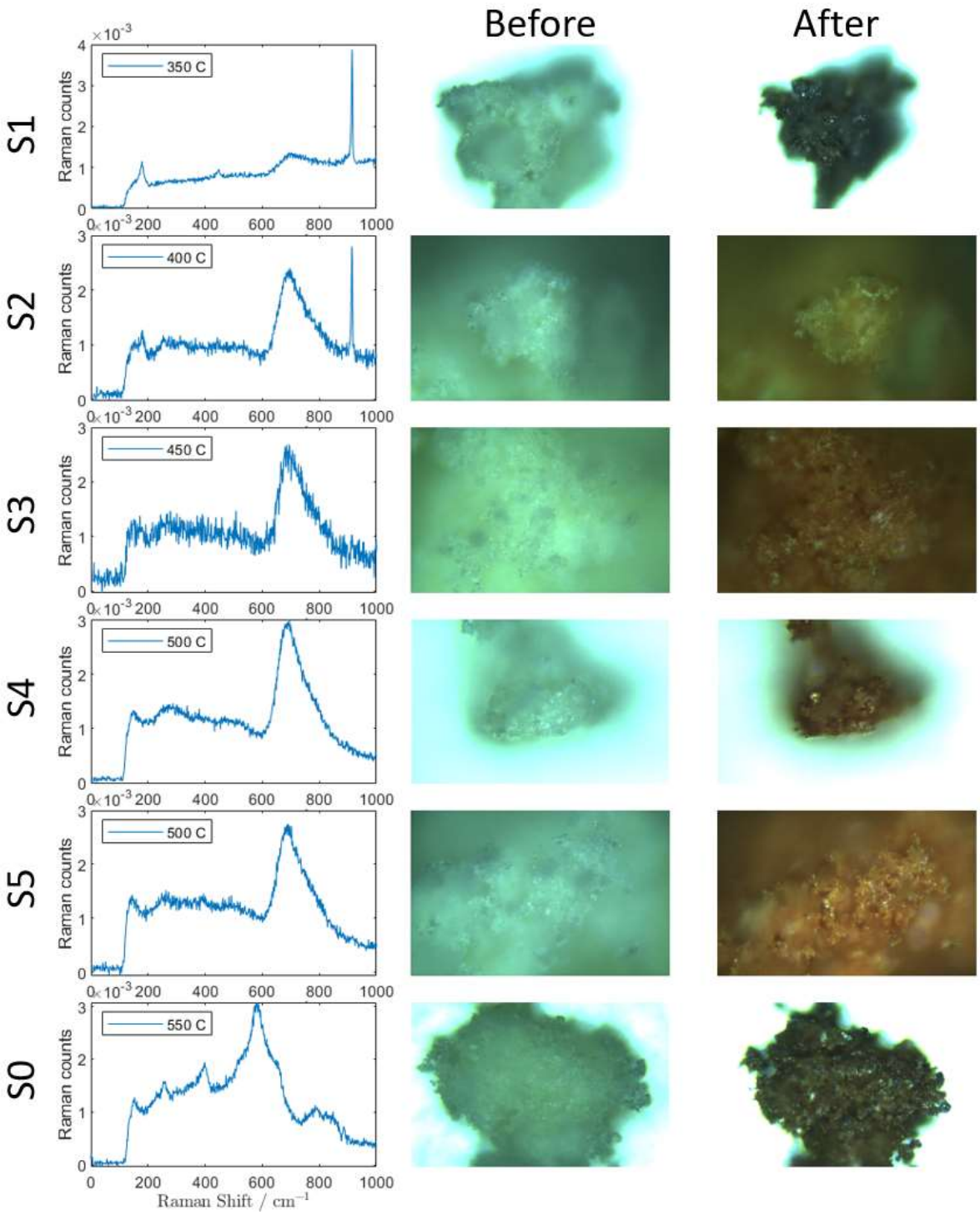

Figure 1. Raman spectra of UO_2F_2 samples after calcination (left), optical image of specimen prior to calcination (middle), and optical image of the same area after calcination (right). Optical images are collected with a 50× long-working length objective (NA = 0.5). The image dimensions are 121 × 97 μm. See text for details on collection of Raman spectra.

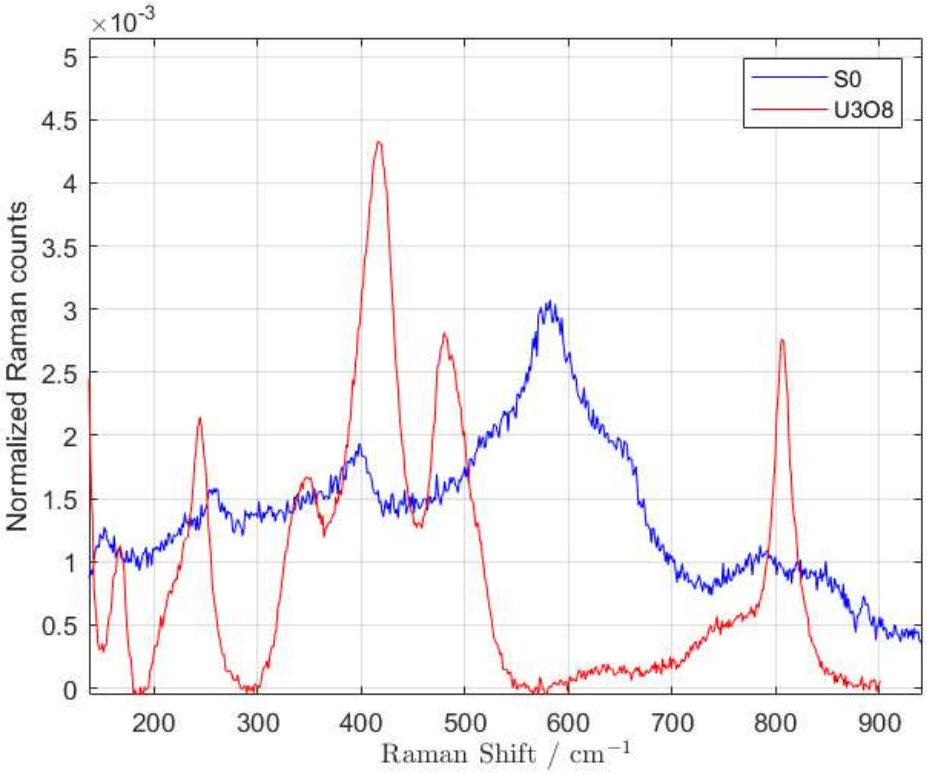

Figure 2. Comparison of Raman spectra of S0 (blue) with spectrum of U_3O_8 (red).

Higher resolution measurements were collected with a 785 nm laser (Figure 3), indicating that the presence of UO_2F_2 persists at least up to 525 °C. Calculating the fraction of UO_2F_2 remaining in S3, S4, S5, and S6 compared to the other samples, the amount of UO_2F_2 is in the ratio 0.44:0.144:0.11:0.15 for S3:S4:S5:S6. It is not possible to directly compare the intensity of the 914 cm^{-1} peak to the intensity of the 680 cm^{-1} peak to determine the phase fractions, but it is clear that uranyl fluoride remains in the sample up to 525 °C and that the quantity is diminishing with increasing calcination temperature, as expected.

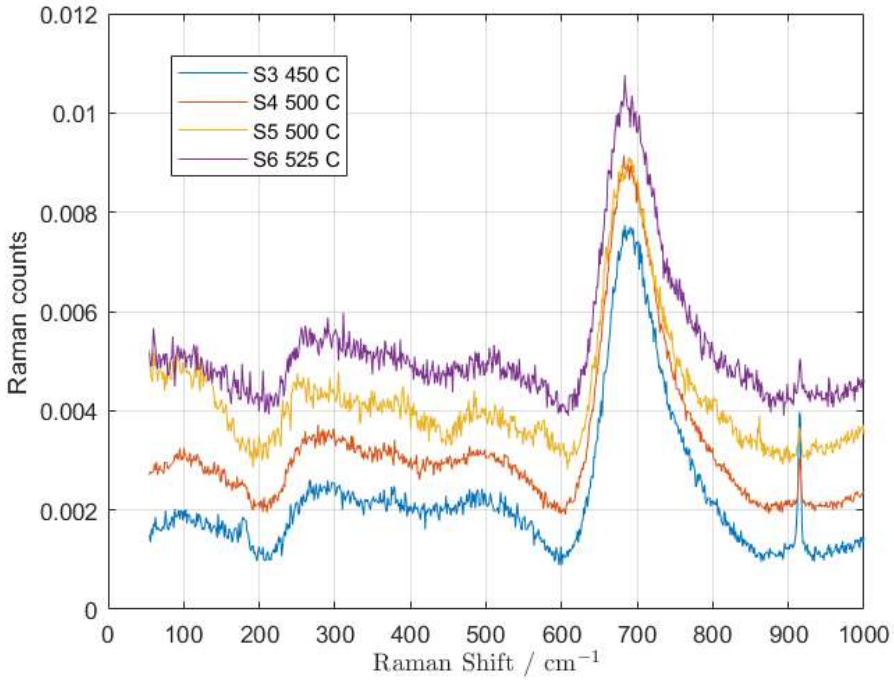

Figure 3. Raman spectra of S3, S4, S5, and S6 collected with the higher resolution (785 nm) setup.

4. SEM MEASUREMENTS

The fluorine content of UO_2F_2 as a function of calcination temperature was investigated via SEM/EDS. An acceleration voltage of 10 kV was employed for EDS measurements and sample topography was analyzed using secondary electron imaging.

Qualitative F/U ratios obtained using EDS were consistent with the results of the Raman spectroscopic investigation; measured fluorine content was lower for UO_2F_2 calcined at higher temperatures (Figure 4, Table 2). In addition, observed F/U ratios differ for samples analyzed using bulk vs. point techniques (Figure 5, Table 2). This suggests that fluorine loss may be heterogeneous and sensitive to sample morphology.

SEM images reveal heterogeneous morphologies for samples treated at lower temperatures, suggesting incomplete calcination and again confirming Raman spectroscopic results. In SEM images of the sample heated to the lowest temperature (350 °C), radiating, fibrous, and subhedral habits are observed, likely related to the presence of both UO_2F_2, and an oxidation product resulting from incomplete calcination (Figure 6). Only subhedral morphologies are present in samples treated at higher temperatures (400–500 °C, Figure 7).

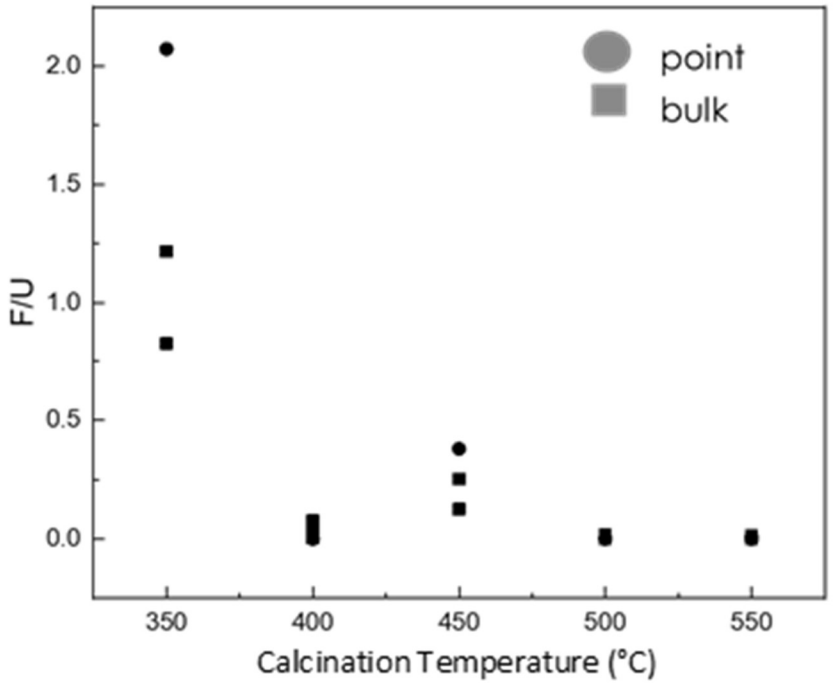

Figure 4. Fluorine-to-uranium ratio plotted as a function of calcination temperature. Increasing calcination temperature resulted in lower F/U.

Table 2. Summary of EDS results.

SAMPLE TEMPERATURE (°C)	MEASUREMENT TYPE	O/U	F/U
350	bulk	2.45	0.82
350	bulk	3.10	1.22
350	point	5.04	2.07
400	point	2.77	0.00
400	bulk	2.26	0.08
400	bulk	1.88	0.00
400	bulk	2.00	0.04
450	bulk	1.65	0.13
450	bulk	2.06	0.25
450	point	3.10	0.38
500	bulk	1.82	0.02
500	point	0.36	0.00
500	bulk	1.61	0.00
500	bulk	1.98	0.00
500	bulk	1.66	0.00
500	point	1.74	0.00
550	bulk	2.70	0.00
550	point	1.97	0.00
550	bulk	0.79	0.01
550	bulk	1.76	0.00
550	point	3.52	0.00
550	bulk	1.67	0.00
550	point	0.98	0.00
550	bulk	2.11	0.01

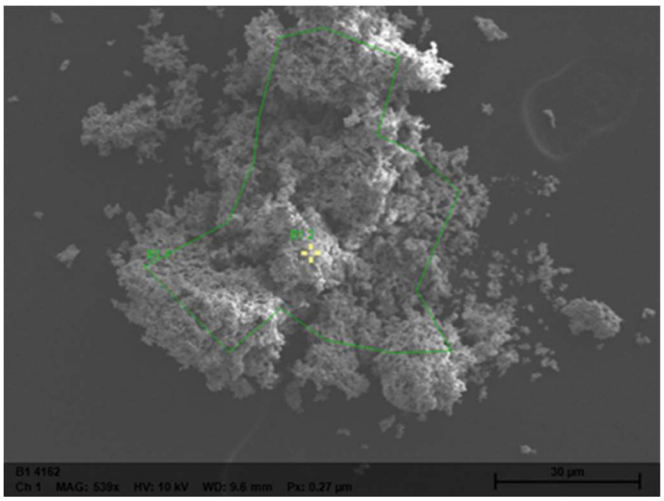

Figure 5. Secondary electron image illustrating the difference between point (yellow reticle) and bulk (green outline) elemental analyses.

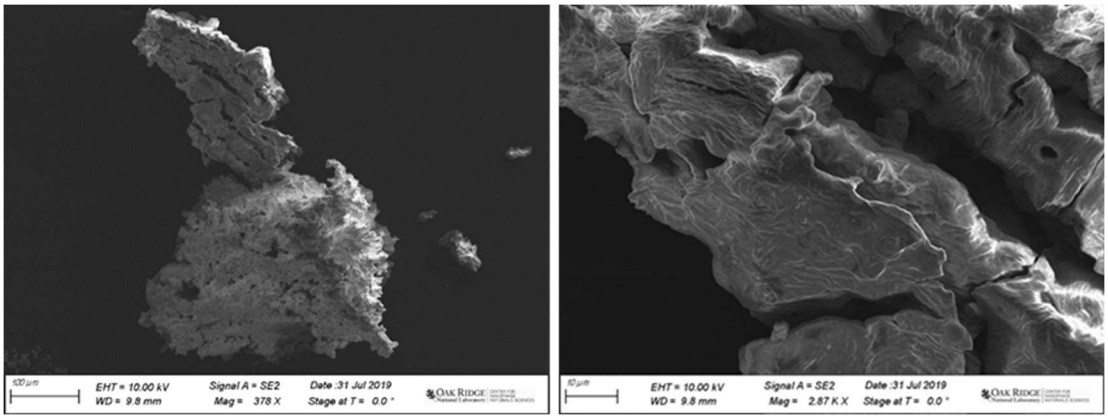

Figure 6. SEM images of two areas on the UO_2F_2 sample heated to 350 °C. Differences in sample morphology are observed (left). Increased magnification of the upper portion of the 350 °C sample (right) reveals a radiating morphology, which differs from the fibrous habit seen on other areas of the sample.

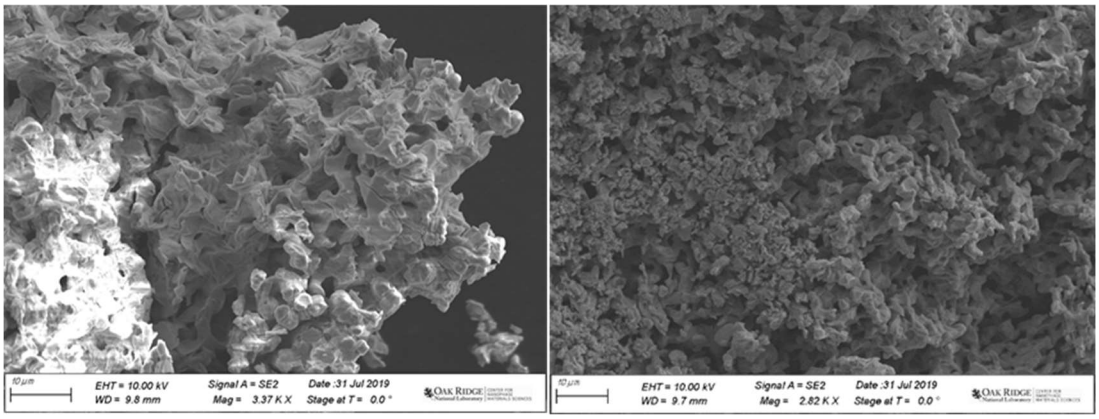

Figure 7. High-temperature samples (400 °C left, 500 °C right) all display similar subhedral morphologies.

5. NANOSIMS MEASUREMENTS

For NanoSIMS analysis, a sub-sample of each calcined UO_2F_2 sample was transferred from the Al crucibles onto a carbon sticky tab using a pair of stainless-steel tweezers that were wiped with an ethanol saturated Kim-wipe between each transfer. All of the UO_2F_2 samples were mounted onto the same carbon sticky tab, with care taken to avoid any cross-transfer between samples. Some of the un-calcined UO_2F_2 starting material was also mounted onto the same carbon sticky tab. After transferring the carbon sticky tab into the NanoSIMS, the instrument was tuned to achieve a mass resolving power of ~7,000 by adjusting the instrument's entrance and aperture slits. Analyses were conducted using a ~200 pA mass filtered $^{16}O^-$ primary beam, with the beam scanned over a 5 × 5 µm area for each analysis. Because the ^{235}U and ^{238}U cannot be collected in the same magnetic field on the NanoSIMS, a magnetic peak hopping approach was used. The peak hopping sequence is provided in Table 3. Each individual analysis consisted of 20 cycles of data, where each of which consists of one sweep through each of the four magnetic fields. During each of these cycles, each mass of interest was counted for ~6.5 seconds. The secondary ion ratios found in Table 4 were computed by calculating the average ratio observed over the final 18 cycles of data generated during each analysis (the first two cycles of data were ignored to allow for the secondary ion signal to stabilize). The uncertainty associated with the ratios in Table 4 is simply the 1σ standard deviation associated with each average. It is important to note that ^{235}U and ^{238}U were collected in

different magnetic fields, however, data from reference materials indicates that this has a negligible effect on the $^{235}U/^{238}U$ ratio under the specific conditions utilized in this study, so no interpolation was performed. Additionally, the raw count-rates were not corrected for the 44 ns detector deadtime, since the effect was determined to be negligible at the relatively low count-rates (in comparison to what is typically observed when substantially higher primary beam currents are used) observed in this study. Lastly, a dataset was also collected on the NIST-610 glass, which was mounted in epoxy and polished down to ¼ micron flatness, to monitor instrument performance. These data are found in Table 4.

Figures 8–12 display the results. In Figures 8 and 9, the $^{235}U/^{238}U$ and $^{19}F/^{238}U$ for the NIST-610 standard demonstrate that the observed $^{235}U/^{238}U$ value agrees well with the published $^{235}U/^{238}U$ (Zimmer et al. 2014) of 0.0023956(5), whereas the observed $^{19}F/^{238}U$ deviates from the assumed F/U ratio (based on a U value of 457 ppm (Pearce et al 1996) and F value of 295 ppm (Hoskin 1998)) of ~0.64. However, the observed $^{19}F/^{238}U$ would be expected to deviate substantially from the true elemental F/U ratio in the NIST-610 glass due to the substantial differences that exist in the secondary ion production characteristics between U and F (e.g., the well-known relative sensitivity effect in SIMS). However, the fact that the $^{19}F/^{238}U$ observed by NanoSIMS is consistent from measurement to measurement and is within the same order of magnitude as the true value suggests that the instrument was performing well during the course of the session within which the calcined UO_2F_2 samples were measured. Examination of the observed $^{19}F/^{238}U$ from the fresh and calcined UO_2F_2 samples (Figure 10) as a function of calcination temperature reveals a progressive decrease in the observed $^{19}F/^{238}U$ with increasing calcination temperature. However, there is considerable variation in the $^{19}F/^{238}U$ observed within each of the calcination batches. This observation is consistent with previous investigations into the behavior of the $^{19}F/^{238}U$ in the uranium matrices. An important observation is that the observed $^{235}U/^{238}U$ for the calcined and fresh UO_2F_2 shows no co-variability with calcination temperature (Figure 11), further suggesting that the instrument was performing in a stable manner. Lastly, observation of the variability in the $^{19}F/^{238}U$ from the fresh and calcined UO_2F_2 samples as a function of the $^{238}U/^{238}U^{16}O$ secondary ion ratios (Figure 12) reveals the same power-law relationship observed in other studies (reference the technical reports). The fact that this power-law relationship is evident in a suite of materials with documented fluorine content variability suggests that the power-law relationship may actually be indicative of real variability in the material, as opposed to an analytical artifact. While this issue is being actively explored in a separate study, another implication is that the observed $^{238}U/^{238}U^{16}O$ variability may also be revealing something about the chemical nature of the material since it appears to vary systematically with the amount of fluorine contained within the calcined materials.

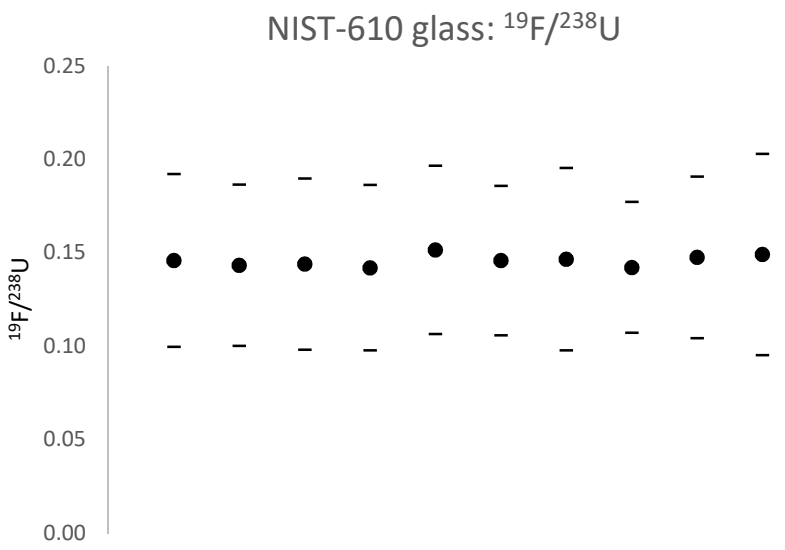

Figure 8. $^{19}F/^{238}U$ ratios for each analysis of the NIST-610 glass.

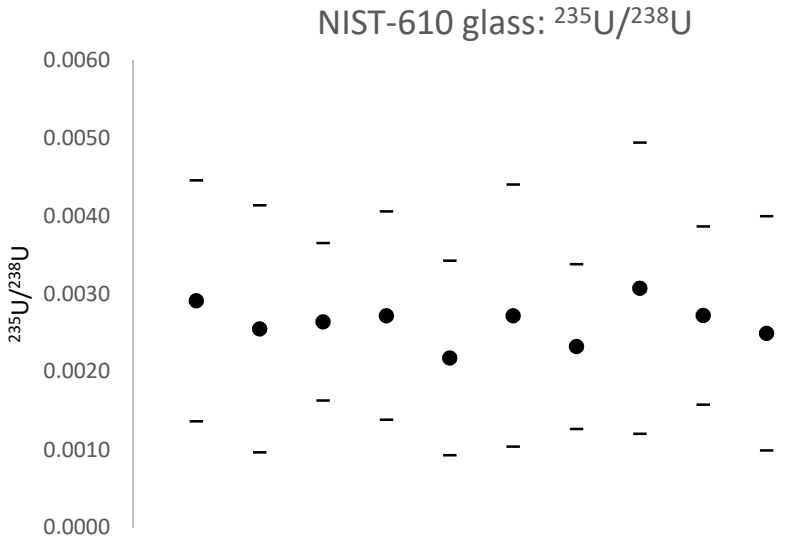

Figure 9. $^{235}U/^{238}U$ for each analysis of the NIST-610 glass.

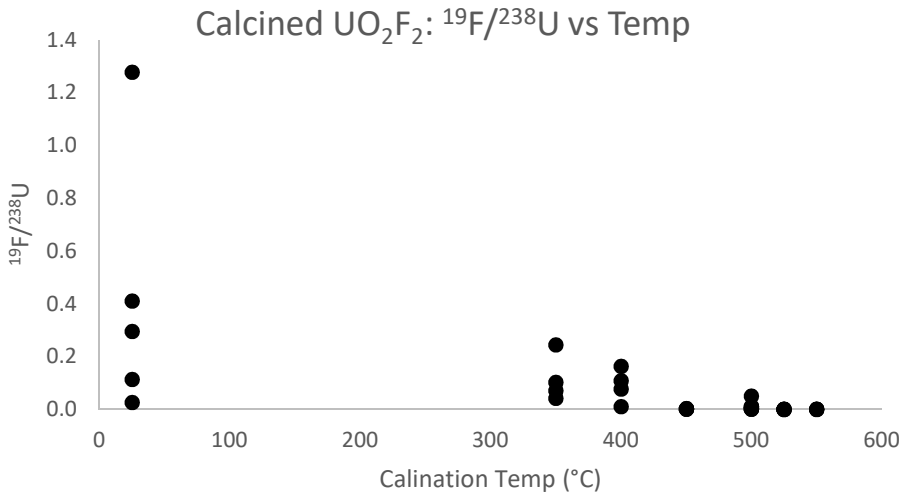

Figure 10. $^{19}F/^{238}U$, plotted as a function of calcination temperature, for each analysis of the fresh and calcined UO_2F_2 samples.

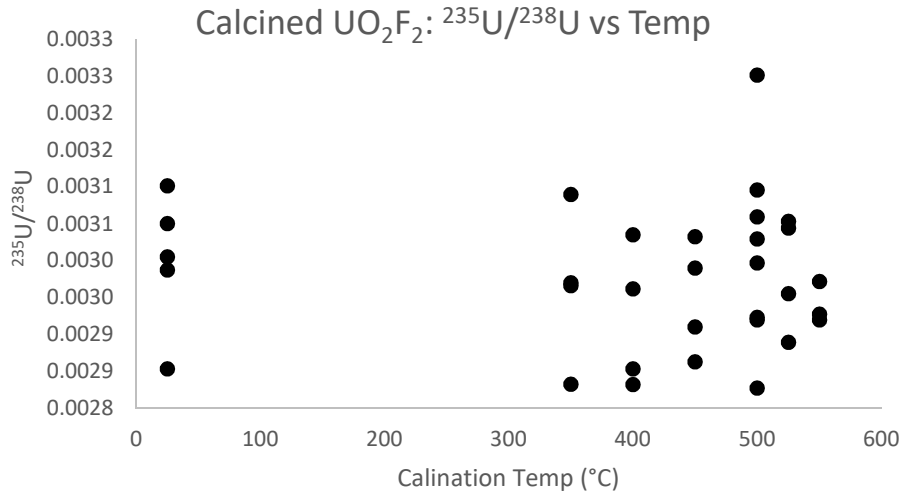

Figure 11. $^{235}U/^{238}U$, plotted as a function of calcination temperature, for each analysis of the fresh and calcined UO_2F_2 samples.

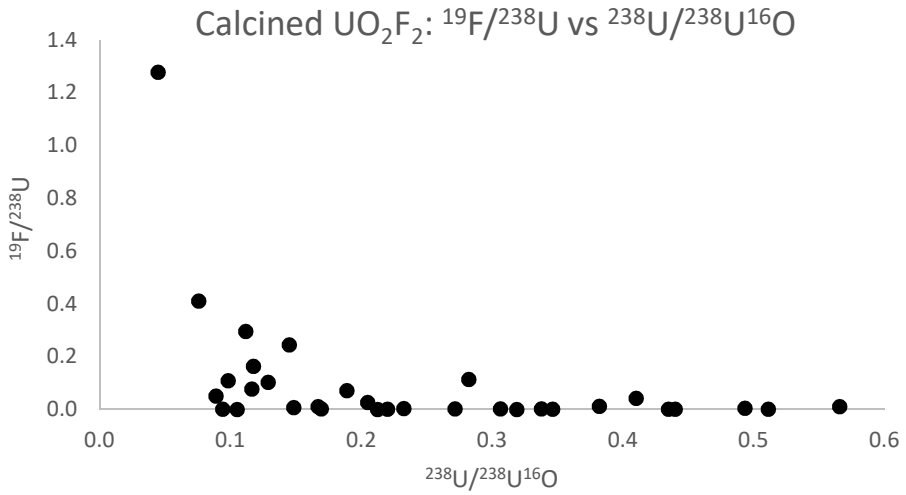

Figure 12. $^{235}U/^{238}U$ vs. $^{238}U/^{238}U^{16}O$, for each analysis of the fresh and calcined UO_2F_2 samples.

Table 3. Detector and magnetic field configuration utilized for analysis of the calcined UO_2F_2 samples. For the purpose of this report, data for the $^{238}U^{19}F$ and $^{238}U^{19}F^{16}O$ secondary ions collected in magnetic field 4 (B4) are not discussed.

	EM1	EM5	EM6	EM7
B1	**settling field**			
B2		^{235}U		
B3	^{19}F	^{238}U	$^{238}U^{16}O$	$^{238}U^{16}O2$
B4			$^{238}U^{19}F$	$^{238}U^{19}F^{16}O$

Table 4. Secondary ion ratios determined according to the procedure described in the text. A full dataset is available upon request.

	$^{235}U/^{238}U$	± 1σ	$^{19}F/^{238}U$	± 1σ	$^{238}U/^{238}U^{16}O$	± 1σ
Calcined 0:						
calcined0_2	0.0030	0.0002	0.0001	0.0001	0.319	0.026
cal0_1f	0.0029	0.0004	0.0004	0.0002	0.440	0.091
cal0_2f	0.0029	0.0002	0.0003	0.0002	0.435	0.097
Calcined 1:						
caclined1_1	0.0028	0.0002	0.0418	0.0074	0.410	0.044
caclined1_2	0.0030	0.0002	0.1027	0.0295	0.129	0.020
cal1_1f	0.0030	0.0003	0.0712	0.0024	0.189	0.005
cal1_2f	0.0031	0.0004	0.2443	0.0273	0.145	0.015
Calcined 2:						
calcined2_1	0.0030	0.0002	0.1089	0.0101	0.098	0.001
calcined2_2	0.0030	0.0003	0.0770	0.0062	0.116	0.003
cal2_1f	0.0029	0.0004	0.1638	0.0216	0.117	0.002
cal2_2f	0.0028	0.0005	0.0106	0.0035	0.566	0.010

Table 4. Secondary ion ratios determined according to the procedure described in the text. A full dataset is available upon request (continued).

	$^{235}U/^{238}U$	± 1σ	$^{19}F/^{238}U$	± 1σ	$^{238}U/^{238}U^{16}O$	± 1σ
Calcined 3:						
caclined3_1	0.0029	0.0003	0.0015	0.0002	0.272	0.053
calcined3_2	0.0029	0.0007	0.0006	0.0005	0.511	0.141
cal3_1f	0.0030	0.0004	0.0020	0.0006	0.306	0.019
cal3_2f	0.0030	0.0003	0.0035	0.0007	0.233	0.021
Calcined 4:						
calcined4_1r	0.0028	0.0002	0.0007	0.0004	0.346	0.024
calcined4_2r	0.0029	0.0002	0.0071	0.0021	0.148	0.041
cal4_1f	0.0029	0.0002	0.0503	0.0065	0.089	0.001
cal4_2f	0.0033	0.0009	0.0104	0.0028	0.167	0.034
Calcined 5:						
calcined5_1r	0.0030	0.0003	0.0022	0.0005	0.169	0.032
calcined5_2r	0.0031	0.0006	0.0016	0.0004	0.338	0.045
cal5_1f	0.0031	0.0002	0.0115	0.0038	0.382	0.086
cal5_2f	0.0030	0.0001	0.0049	0.0021	0.493	0.149
Calcined 6:						
calcined6_1r	0.0029	0.0002	0.0011	0.0005	0.220	0.042
calcined6_2r	0.0030	0.0004	0.0002	0.0001	0.212	0.039
cal6_1f	0.0031	0.0008	0.0002	0.0001	0.105	0.003
cal6_2f	0.0030	0.0002	0.0003	0.0001	0.094	0.001
UO_2F_2 produced June 2019:						
freshUO_2F_2_2	0.0029	0.0002	0.1141	0.0236	0.282	0.066
freshUO_2F_2_3	0.0030	0.0004	0.4106	0.2830	0.076	0.014
freshUO_2F_2_4	0.0031	0.0002	1.2775	0.2080	0.045	0.000
freshUO_2F_2_1f	0.0030	0.0002	0.2957	0.0109	0.112	0.003
freshUO_2F_2_2f	0.0031	0.0005	0.0262	0.0075	0.205	0.003
NIST-610 glass:						
Aug19_NIST610_1	0.0029	0.0015	0.1459	0.0462	0.435	0.013
NIT610_2	0.0026	0.0016	0.1434	0.0432	0.443	0.013
NIST610_3	0.0026	0.0010	0.1439	0.0457	0.438	0.013
NIT610_4	0.0027	0.0013	0.1420	0.0443	0.441	0.012
NIST610_5	0.0022	0.0012	0.1516	0.0450	0.440	0.009
Aug20_NIST610_1	0.0027	0.0017	0.1459	0.0400	0.427	0.012
Aug20_NIST610_2	0.0023	0.0011	0.1466	0.0488	0.434	0.015
Aug20_NIST610_3	0.0031	0.0019	0.1422	0.0350	0.430	0.012
Aug20_NIST610_4	0.0027	0.0011	0.1476	0.0432	0.431	0.017
Aug20_NIST610_5	0.0025	0.0015	0.1491	0.0538	0.428	0.014
Mixed LaF_3-UO_2/U_3O_8 powders:						
$LaFU_3O_8$_1	0.0023	0.0001	0.0277	0.0048	0.195	0.020
$LaFU_3O_8$_2	0.0023	0.0002	0.0194	0.0031	0.264	0.012
$LaFUO_2$_1	0.0022	0.0005	0.0584	0.0111	0.212	0.012
$LaFUO_2$_2	0.0022	0.0002	0.1560	0.0154	0.152	0.009

6. DISCUSSION & PROSPECTS

This research pursued several avenues simultaneously. They were: First, investigate the calcination behavior of uranyl fluoride. Second, study the analytical effect of calcination on NanoSIMS measurement. Third, investigate the feasibility of a mixed powder material as a high F, high U standard material.

Based on Raman spectra results and chemical intuition, the calcination of UO_2F_2 appears to proceed to U_3O_8 beginning no later than 350 °C with a very wide transition range (the primary product after calcination for 1 hr at 550 °C remains a species other than U_3O_8). A more full investigation of this transition requires *in situ* x-ray diffraction and a wider temperature range. It was intended to maintain a small quantity of specimen for this study for the purposes of reducing morphological effects on surface reactions; unfortunately, this consideration precludes the measurement of post-facto x-ray diffraction patterns which typically require mg quantities of material. Accessing temperatures above 550 °C requires specialized equipment due to the proclivity of most materials to rapidly oxidize; but, it is a valid scientific goal to understand the phase transition kinetics of the calcination of uranyl fluoride.

The NanoSIMS results suggest that more study on samples of known F/U ratio should be performed. If it is the case that UO_2F_2 demonstrates high intrinsic elemental ratio variability, it is necessary to increase confidence in the analytical stability of the measurement. Therefore, not only is a bulk (average) F/U ratio measurement necessary, it is also necessary to understand elemental variations on the NanoSIMS analytical length scale (microns). In other words, a secondary measurement of F/U ratio in the same analytical volume is a direct method to gain confidence in the measured results. An indirect method for increasing confidence in the analytical method is to generate statistical distributions of F/U ratio and compare them to statistical distributions measured on comparable samples with a distinct method. In principle, the demonstration here is of the latter type, whereby measurement of the F/U ratio via SEM/EDS is compared in kind to the F/U ratio collected with NanoSIMS.

It was intended to compare the F/U ratio collected via SEM/EDS and NanoSIMS to a second, analytical method of determining F/U, such as inductively coupled plasma mass spectrometry (ICP-MS) or ICP-optical emission spectrometry (ICP-OES). Although it became apparent that the micron-scale variations in F/U may be of higher relevance than the bulk F/U ratio, a measurement of the bulk F/U ratio remains valuable. It became apparent that additional method development would be required to measure the F/U ratio with either approach, requiring a dedicated research thrust. It is recommended that such an analytical capability be expanded in support of further investigation into micron-scale F/U variations.

One goal of this set of experiments was to investigate the lower fluorine concentration sensitivity limits of the NanoSIMS. It was expected that samples of UO_2F_2 would completely oxidize at 550 °C (the maximum accessible calcination temperature with the variable temperature stage), but even the S0 sample showed a significant concentration of F compared to the NIST glass standard (itself <100 ppm F). Therefore the question of lower concentration limits could not be explored with this set of samples.

Finally, it will be necessary to produce standard materials of known F/U ratio, with the property that they be elementally and isotopically homogeneous, chemically stable, and relatively easy to prepare. Although standards containing both F and U exist, their concentrations (<100 ppm) are not appropriate to compare to UO_2F_2 specimens wherein the F and U concentrations are expected to be at molar concentrations. An initial attempt was made to investigate the feasibility of a mixed powder of LaF_3 and U_3O_8, which are stable and homogenous. The elemental concentrations of LaF_3 and U_3O_8 could theoretically be varied simply by changing the bulk mass of the mixed powders. It was found that the spatial variation of the elemental compositions was too significant to be used as a reference material, as is indicated by the spread in $^{19}F/^{238}U$ values listed in Table 4. Although this result was unsurprising, it was valuable to

investigate the possibility as the prospect of producing mixed powder standards is very attractive. A promising next step is the formation of fluoride-based glass materials. In particular, we noted the chemical similarity between ZrF_4 in ZBLAN fluoride-based optical glass (used commercially in fiber optic applications) and UF_4. ZrF_4 and UF_4 are isomorphic, having the same crystal structure, and so it is speculated that substitution of UF_4 for ZrF_4 could be feasible and allow for the synthesis of a variety of F/U concentrations. Some precedent for the production of U-containing fluoride glasses exists. Another possibility is the formation of amorphous glasses involving the fusion of a U-bearing compound of relatively low melting point with a fluorine-based glass precursor. Additional synthesis capability is necessary to pursue these possibilities. In particular, melting fluorine glass typically requires furnaces with controlled atmosphere to prevent rapid oxidation and loss of fluorine.